PHYSICS OF EARTH, ATMOSPHERE, AND HYDROSPHERE

The Influence of the Duration of Wind Impact on the Formation of Currents and a Thermal Bar in a Freshwater Reservoir over the Period of Melting of the Ice Cover

N. S. Blokhina*

Department of Physics, Moscow State University, Moscow, Russia
*e-mail: blokhinans@gmail.com
Received September 26, 2017; in final form, October 17, 2017

Abstract—The impact of wind of different strengths, directions, and durations on the development of a thermal bar and accompanying currents in reservoirs over the period of ice cover melting was studied using mathematical modeling. It is shown that as the duration of the wind impact on the reservoir increases, the role of energy exchange at the water-air interface in the formation of currents in the reservoir increases. The passage of surface waters through the temperature of maximum density (4°C) leads to the formation of a thermal bar and convective structures to the right and to the left of it. In this case, the increase in the energy exchange as the duration of the wind grows occurs with different degrees of intensity on different sides of the thermal bar. In certain hydrometeorological situations (when the wind is directed offshore) this can increase the intensity of the convective vortex in the deep part of the reservoir and weaken it in the shore part, which will slow the propagation of the thermal bar towards the center of the reservoir.

Keywords: mathematical modeling, thermal bar, temperature of maximum density, wind, energy exchange, ice cover.

DOI: 10.3103/S0027134918040045

INTRODUCTION

In freshwater lakes at northern latitudes, one feature of the formation of the currents in the spring is associated with the generation and development of a thermal bar (TB) under conditions of ice-cover melting [1−4]. A thermal bar occurs in the ice-free part of a reservoir where the surface waters are heated to the temperature of the maximum density. In freshwater reservoirs, this is $T_{max} = 4°C$. The surface waters that reach this temperature become the heaviest and descend to the bottom, forming a frontal division from the surface to the bottom with the temperature of 4°C, that is, a thermal bar (Fig. 1). To the right and to the left of the thermal bar, convective structures that cover near-shore and deep waters occur, respectively. Here, as follows from in-situ observations [1, 2, 4], a deep convective vortex spreads over subglacial and ice-free waters. While the reservoir is heated and ice melts the thermal bar moves forward to the reservoir center parallel to the shore and disappears when the temperature of surface waters exceeds $T_{max} = 4°C$. In deep reservoirs, it can exist for several months, making a major contribution to the formation of thermohydrodynamic processes. By restricting energy and substance exchange between the near-shore and deep waters, the thermal bar exerts a considerable impact on the eco-

logical state of the reservoir [5, 6]. The presence of an ice cover in the reservoir during the existence of the TB adds its own features to the formation of the currents. Therefore, the study of thermal and dynamic processes in reservoirs during melting of the ice cover is of great scientific and practical interest.

From the time when a thermal bar was observed for the first time by F.A. Forel [7], A.I. Tikhomirov [8, 9], and G.K. Rodgers [10] in different world lakes to the and was explained by A.I. Tikhomirov from the physical point of view [8], a lot of in-situ observations were performed and laboratory. Moreover, mathematical models were constructed to explain the dynamics of the development of a thermal bar. References to some of these works were given in a review in [5]. However, there are only a few studies on the influence exerted by the different hydrometeorological conditions on the formation of a thermal bar. The in-situ observations that describe the initial stage of the formation of a thermal bar near the shore during ice melting were presented in [1, 2]. The mathematical model that describes the development of a thermal bar and accompanying currents in this period was presented in [11]. Wind has also a special effect on the formation of currents in reservoirs. Its effects on the thermohydrodynamic processes and thermal-bar development in ice-free reservoirs in the spring, fall, and over the

period of ice melting (during a short-time wind impact on the reservoir) were studied in [12−16], [17], and [18−20], respectively.

Using mathematical modeling, we studied the features of the development of a thermal bar and currents in a reservoir during melting of the ice cover under conditions of the long-term impact of the wind on the water surface.

FORMULATION OF THE PROBLEM

Because a thermal bar front in a reservoir is directed parallel to the shore (along the X_1 axis) (Fig. 1) and the motion of the water in this direction is homogeneous, we solved the 2D problem in the $X_2 X_3$ plane.

We considered the motion of a viscous incompressible liquid in half of the reservoir (Fig. 1), which is symmetrical relative to the X_3 vertical axis. The X_2 axis is directed towards the shore. The depth of the reservoir is equal to H and the widths over the surface and the bottom equal L_1 and L, respectively. In the central part of the reservoir ice H_1 thick and L_3 long (along the X_2 axis) was located. The wind blew over the reservoir along this axis at the velocity V with opposite orientations (towards the shore and away from it) and strengths.

We used a mathematical model created in [11, 18, 21−22] to model thermohydrodynamic processes in the reservoir during development of a spring thermal bar.

We solved a system of Navier−Stokes equations in the Boussinesqu approximation and the equation of thermal conductivity. The anomalous dependence of the water density on the temperature at approximately 4°C was assigned as

$$\rho(T) = \rho_o(4°C) - \rho_o(4°C)\gamma(T - 4°C)^2. \tag{1}$$

Here, T is the temperature, ρ is the water density, ρ_o is the water density at 4°C, and $\gamma = 0.000085°C^{-2}$.

Since the water motion is homogeneous along the thermal bar front, we considered a planar problem. Here, the equation of continuity permitted the introduction of the stream function ψ.

We wrote the system of thermohydrodynamic equations in the variables of the stream function ψ and the vortex φ in the dimensionless form (below φ, ψ, and T denote the dimensionless variables):

$$\frac{\partial \varphi}{\partial t} + \left(\frac{\partial \psi}{\partial x_3}\frac{\partial \varphi}{\partial x_2} - \frac{\partial \psi}{\partial x_2}\frac{\partial \varphi}{\partial x_3}\right)$$
$$= \mu\left(\frac{\partial^2 \varphi}{\partial x_2^2} + \frac{\partial^2 \varphi}{\partial x_3^2}\right) - 2(T - T4)\frac{\partial T}{\partial x_2}, \tag{2}$$
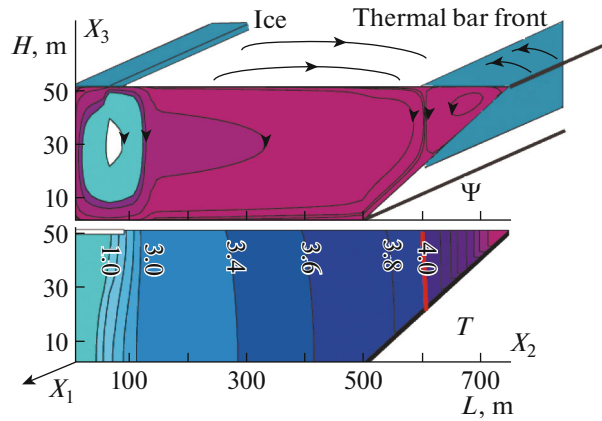
Fig. 1. The scheme of the water reservoir. The field of the distribution of the temperature T and the flow function ψ in the reservoir that was still ice covered in the phase of origination of the thermal bar near the shore.

$$\frac{\partial T}{\partial t} + \left(\frac{\partial \psi}{\partial x_3}\frac{\partial T}{\partial x_2} - \frac{\partial \psi}{\partial x_2}\frac{\partial T}{\partial x_3}\right) = \mu\left(\frac{\partial^2 T}{\partial x_2^2} + \frac{\partial^2 T}{\partial x_3^2}\right), \tag{3}$$

$$\Delta\psi = \varphi. \tag{4}$$

Here, $\mu = \nu_T/H\sqrt{gH}$ is the dimensionless coefficient of exchange and $T4$ is the dimensionless value of the temperature of the freshwater maximum density. In introducing dimensionless variables, we accepted the following scales for the values: the dimension $L_m = H$; the velocity $V_m = \sqrt{gH}$; the time $t_m = \sqrt{(H/g)}$; and the temperature $T_m = 1/\sqrt{\gamma}$. Here, H is the reservoir depth, g is the acceleration of gravity, and γ is a coefficient in formula (1).

To close the system of equations (1−4), we introduced the coefficient of turbulent viscosity ν_T, which was calculated by using the ratio $\nu_T = C\varepsilon^{1/3}H^{4/3}$ [23].

The dissipation rate of the turbulence energy ε was found from the equation of the turbulence energy balance. In the dimensionless form, the closing equation had the form

$$\mu^2 = \frac{C^3}{s}$$
$$\times \int_s \left[4\left(\frac{\partial^2 \psi}{\partial x_2 \partial x_3}\right)^2 + \left(\frac{\partial^2 \psi}{\partial x_3^2} - \frac{\partial^2 \psi}{\partial x_2^2}\right)^2 - (T - T4)\frac{\partial T}{\partial x_3}\right]ds, \tag{5}$$

where s is the area of the region of the problem solution and C is an empirical coefficient.

The boundary conditions for the system of equations were written as follows. At the bottom of the reservoir and the right sloping lateral boundary, the con-

ditions of adhesion and impermeability for the velocity and the absence of heat flux were:

$$\frac{\partial \psi}{\partial x_2} = \frac{\partial^2 \psi}{\partial x_3^2} = 0, \quad \frac{\partial T}{\partial x_3} = 0 \quad \text{and}$$

$$\frac{\partial \psi}{\partial n} = \frac{\partial^2 \psi}{\partial n^2} = 0, \quad \frac{\partial T}{\partial n} = 0. \tag{6}$$

respectively. Here, n is the normal to the sloping lateral boundary.

At the left boundary, the condition of symmetry for all variables is:

$$\frac{\partial T}{\partial x_2} = 0, \quad \psi = 0, \quad \varphi = 0. \tag{7}$$

At the upper boundary, for the part of the ice-free reservoir these are:

$$-\mu \frac{\partial T}{\partial x_3} = Q_b, \quad \frac{\partial \psi}{\partial x_2} = 0,$$

$$\varphi = \frac{\partial^2 \psi}{\partial x_3^2} = \tau_b = \frac{C_D \rho_a V_b^2}{\rho_0 \mu}; \tag{8}$$

under the ice these are:

$$\frac{\partial \psi}{\partial x_2} = \frac{\partial^2 \psi}{\partial x_3^2} = 0, \quad T = 0. \tag{9}$$

Here, ρ_a is the air density, C_D is the coefficient of friction, τ_b is the dimensionless stress value of wind friction, and $Q_b = Q_r + Q_L + Q_1$ is the dimensionless heat flux. The value $Q_1 = \sqrt{\gamma}/c_o \rho_o \sqrt{gH}$ was accepted as the scale of flux.

The dimensionless heat fluxes were calculated from the formulas:

$$Q_T = \rho_a c_p C_T (T - T_{air}) V / Q_1 \tag{10}$$

for the sensible heat flux,

$$Q_L = L C_q (q - q_{air}) V / Q_1 \tag{11}$$

for latent heat flux, and

$$Q_i = \delta \sigma (273.15 + T)^4 / Q_1 \tag{12}$$

for the long-wave radiation flux.

In these expressions, c_p and c_o are the heat capacities of the air and water at constant pressure, C_T and C_q are the Stanton and Dalton numbers for the transfer of heat and moisture, L is the latent heat of evaporation, T_{air} and q_{air} are the temperature and specific humidity of the air, and T and q are the temperature of the water surface and the specific humidity near its surface: $\sigma = 5.67 \times 10^{-8}$ W/(m$^2 \times$ K^4); $\delta = 0.95$.

The dimensional expression for the latent heat flux (11) versus the temperature of the underlying surface T can be written with respect to the relative humidity of

the air f and the dependence of the saturating humidity on the air temperature in the form:

$$q = \Phi(T) = \Phi(T_{air} + (T - T_{air}))$$

$$= \Phi(T_{air}) + \frac{\partial \Phi}{\partial T}(T - T_{air}).$$

Here, we took into account the fact that the difference of the water–air temperature is usually small, which makes it possible to linearize the expression for q near the value of the air temperature.

We represent the specific air humidity as $q = f^*\Phi(T_{air})$. Then,

$$Q_L = \left(L C_q ((1 - f)\Phi(T_{air}) + \frac{\partial \Phi}{\partial T}(T - T_{air}))V \right) / Q_1. \tag{13}$$

The thickness of the ice cover H_i is found from the equation

$$\frac{\partial H_i}{\partial t} = \frac{(Q_{WB} + Q_{WL} + Q_2)}{L_i r_i}, \tag{14}$$

where L_i is the specific heat of ice melting, r_i is the ice density, and Q_{WB} and Q_{WL} are the flows coming to the bottom and lateral ice boundaries from the water, respectively. $Q_2 = Q_R + Q_i$, where Q_R is the radiation heat flux from the sun and Q_i is the long-wave radiation flux from the ice surface.

The problem was solved numerically. The system of equations (2)–(4), the boundary conditions (6)–(9), the equation of closing (5), and the ice-balance equation (14) were represented in the finite-difference form using central differences for the approximation of the spatial and one-sided differences for time derivatives. We used an explicit finite-difference scheme. The Poisson equation was solved by the method of successive over-relaxation [24]. The calculations were performed on a 26 × 76 mesh. The mesh step was 2 m in the vertical direction and 10 m in the horizontal direction.

THE PARAMETERS OF THE PROBLEM

We considered a reservoir with the depth $H = 50$ m and the width $L_1 = 750$ m (half of the reservoir). The wind velocity took the values $V = 1, 3, 5,$ and 7 m/s. The wind direction was assigned on and offshore. The atmosphere temperature was accepted equal to $T_a = 8°C$ and the relative air humidity $f = 60\%$. The solar radiation flux to the reservoir surface $Q_R = 450$ W/m^2. The wind impact on the water surface lasted up to 15 h. The initial fields of distribution of the temperature (T) and the stream function (ψ), as well as the vortex field (φ) correspond to the case where a near-shore thermal bar was formed in the reservoir in the spring. The central area of the reservoir is ice covered and an
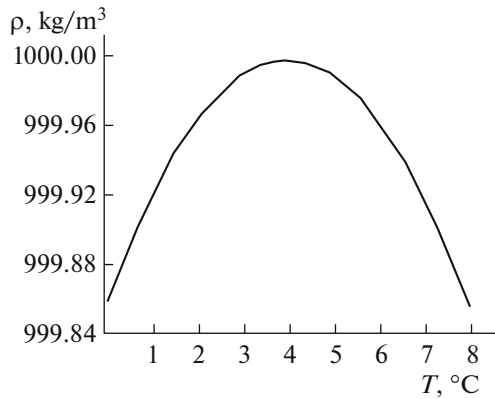
Fig. 2. The dependence of the water density ρ on the temperature T around 4°C.

intense deep vortex (IDV) was formed near its margin [11]. The initial fields of T and (ψ) coincide qualitatively with the fields in Fig. 1.

RESULTS AND DISCUSSION

In the spring, a thermal bar (a frontal interface, TB) is generated near the shore in reservoirs that are free of ice and are still ice-covered. Convective structures that converge along the frontal division and cover the near-shore and deep waters are formed to the right and to the left of it. Here, in the second case, a vortex structure originates near the ice margin (inside the anticyclonic vortex to the left of the TB), where a considerable temperature gradient is observed along the horizontal direction (Fig. 1) [11].

The origination of this vortex is caused by the maximum water density (ρ_{max}) at $T_{max} = 4°C$ (Fig. 2). The water density increases at 0 to 4°C and decreases at 4 to 8°C in the same way. Its highest gradient is recorded far from $T_{max} = 4°C$.

The criterion of convective instability of water masses is the dimensionless Grashof number Gr. For anomalous dependence of the fresh water density on the temperature, it has the form $Gr = \dfrac{g\gamma\Delta T^2 H^3}{\nu^2}$ [25]. Here, g is the acceleration of gravity, γ is the coefficient in formula (1), ΔT is the difference of the temperatures between the reservoir surface and bottom, ν is the kinematic viscosity, and H is the reservoir depth.

The greater the Grashof number is, the more unstable the water layer is and the more intensive the convection is. At the ice margin (Fig. 1) and the thermal bar (to the left of it), the surface−bottom temperature differences equal $\Delta T_1 \approx 0.3°C$ and $\Delta T_2 \approx 0.06°C$, respectively.

In this situation, the ratio of the Grashof numbers $Gr_1/Gr_2 \sim 25$. The greatest density instability of water masses is recorded near the ice margin, which leads to

origination of a convective structure inside that covers the reservoir from the center to the TB of the intense deep vortex (IDV).

After the ice melts, the water temperature increases over the entire water area of the reservoir, approaching $T_{max} = 4°C$ to the left of the TB and exceeding it in the near-shore region. The density of deep waters (to the left of the TB) tends to the maximum value, while the density of the near-shore waters decreases (Fig. 2). This leads to an increase in the instability of the surface waters to the left of the TB, an increase in the size of the IDV, to its distribution to the TB and intensification of circulation in the deep area of the reservoir. The further heating of the water can intensify deep circulation even more for some time, which decelerates the TB motion away from the shore [20].

Wind blowing over the water area of the reservoir can change the described pattern of the currents. First of all, the zone of convergence of the vortices and the thermal bar (in classic understanding of the frontal interface with the temperature $T_{max} = 4°C$ from the surface to the bottom) may not coincide. This depends on the reservoir depth, the wind velocity, and its direction [18, 19]. Under natural conditions, a discrepancy between the regions of water convergence on the surface and the 4°C isotherm was observed near the east coast of Lake Ladoga (the data of observations by S.G. Karetnikov and M.A. Naumenko were given via oral communication by M.A. Naumenko). Further, we will discuss the wind impact on the formation of the zone of vortex convergence over the period of ice-cover melting. The studies were performed for the cases of wind direction on and offshore for different durations of wind impact on the reservoir surface.

The analysis of the results for the case of the wind directed offshore showed that when the wind velocity increases and the duration of the wind impact on the water surface is the same, the zone of vortex convergence moves to the reservoir center at a greater velocity. This is quite natural, since both the wind impact and reservoir heating contribute to the motion of the near-shore circulation off the shore. The situation where the wind is directed offshore at the same wind velocity and different durations of its impact on the reservoir is interesting (Fig. 3). Figure 3 presents the fields of the distribution of the temperature T and the stream function ψ at the wind velocity $V = 5$ m/s $t = 1$, 3, and 6 h after the onset of the impact. The longer the wind blew, the slower the zone of vortex convergence moved towards the reservoir center. At first glance, this is an untypical situation. Here, both the wind and density instability act in the same direction during heating of the near-shore surface waters to the temperature of maximum density, contributing to the movement of the zone of vortex convergence away from the shore. During wind impact on the water area of the reservoir this phenomenon is explained not only
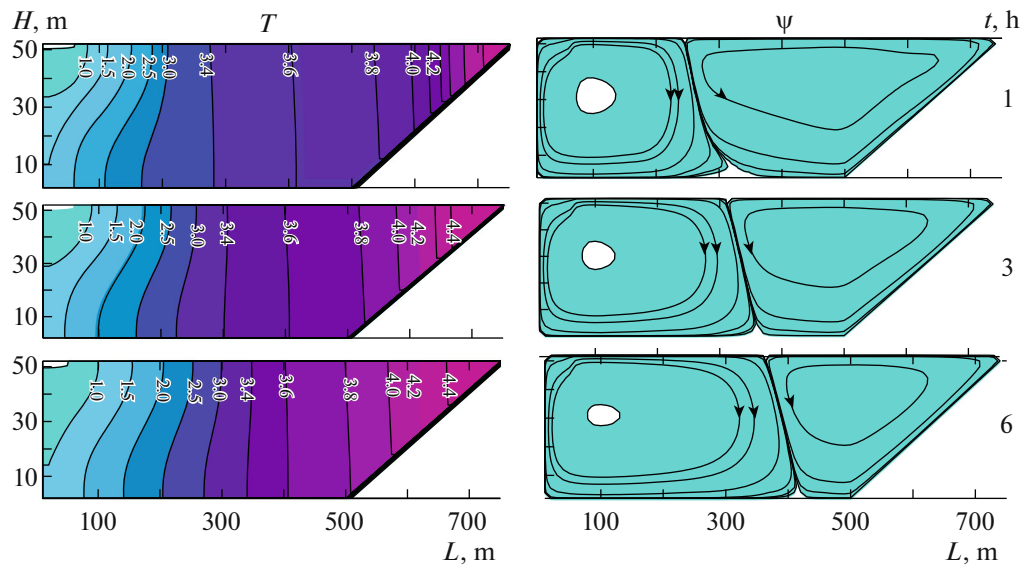
Fig. 3. The fields of the distribution of the temperature T and the stream function ψ under the offshore wind ($V = 5$ m/s), $t = 1$, 3, and 6 h after the onset of the wind impact on the reservoir.

by the anomalous water properties [20], but also by the increased energy exchange at the reservoir–atmosphere interface. The longer the wind is blowing and the greater its velocity is, the larger the fluxes of the sensible (11) and latent (13) heat are, which contribute to the change in the water temperature. This also leads to a change in the flux of longwave radiation (12) that cools the surface waters.

When the TB is in the reservoir, it divides the surface waters into warmer $T > 4°C$ (to the right of the TB) and cooler $T < 4°C$ (to the left of the TB). Here, we observe the regions of the maximum horizontal temperature gradients in the water and the air that move along the reservoir surface following the TB motion and vanish when the temperature of the surface waters of 4°C is exceeded [26, 27]. In certain hydrometeorological situations this will lead to a change in the direction of the total heat flux at the reservoir–atmosphere interface [28]. On one side of the TB, the waters may be heated, on the other side they are cooled. When the wind impact on the reservoir is longer, its surface waters are heated for a longer time, which contributes to the change in the energy exchange between the reservoir and the atmosphere with different degrees of intensity in different parts of the reservoir.

Under the meteorological conditions considered in this work, on the one hand, the sensible heat flux from the reservoir grows due to evaporation (primarily in the warm near-shore area), which leads to a decrease in the water temperature. On the other side, the latent heat flux increases in the direction to the reservoir (primarily in the cold central part of the reservoir), which leads to heating of the water. This changes the temperature of the surface waters and, consequently,

the flux of longwave radiation (formula (12)), which contributes to the cooling of the reservoir. The total impact of the heat fluxes on the reservoir results in faster heating of the near-shore waters. Their temperature increasingly exceeds $T_{max} = 4°C$, which leads to a decrease in the water density (Fig. 2). The deep waters remain cooler than 4°C and their density approaches maximum with time. This contributes to the additional intensification of deep circulation. As a result, the zone of vortex convergence and the near-shore circulation start to move more slowly to the reservoir center. The situation changes with time. The longer duration of a wind impact on the reservoir leads to a change in the temperature of the surface water, so that the near-shore waters become more unstable near the shore and the near-shore circulation starts to displace the deep circulation.

When the wind is directed at the shore, the density instability and the drift current influence the reservoir in different directions. In the deep reservoir that is considered in this work the adsorption of the near-shore circulation by the deep circulation occurs approximately equally in these two situations. In the first situation, this occurs at a great wind velocity V and a short time t of its impact on the water surface (Fig. 4a; $V = 7$ m/s, and $t = 1$ h); in the second situation, this occurs at small values of V and a longer wind impact on the reservoir (Fig. 4b; $V = 3$ m/s, and $t = 6$ h). In the first case, its disappearance occurs primarily due to the drift current. In the second case, it occurs due to the duration of the reservoir heating. As we showed above, the anomalous property of fresh water and the change in the energy exchange between
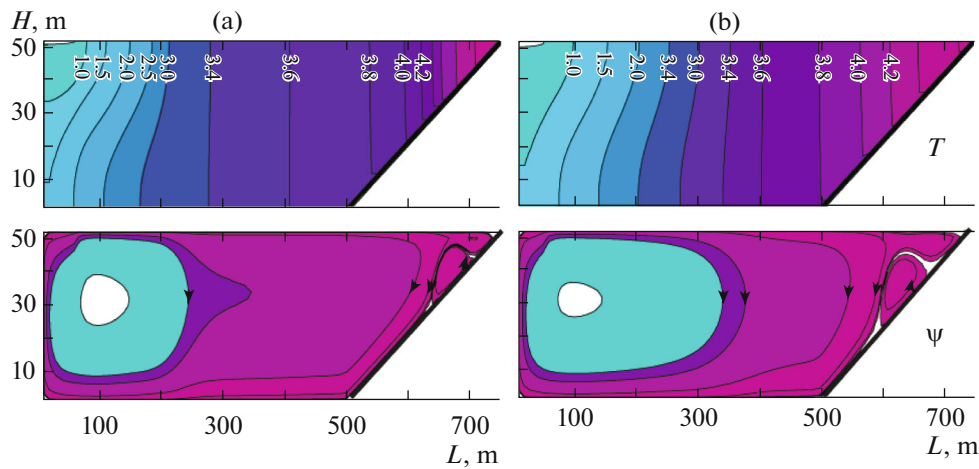
Fig. 4. The fields of the distribution of the temperature T and the stream function ψ in the reservoir during an onshore wind. a—the wind velocity $V = 7$ m/s, $t = 1$ h; b—$V = 3$ m/s, $t = 6$ h.

the reservoir and the atmosphere causes an increase in the intense deep vortex. In approaching the shore and combining with the vortex structure to the left of the thermal bar, the intense vortex structure suppresses the near-shore circulation.

CONCLUSIONS

These studies showed that over the period of ice cover melting, the development of the thermal bar and the accompanying currents significantly depends not only on the wind strength and direction, but also on the duration of its impact on the reservoir. The longer the wind is blowing, the greater the role that is played in formation of currents by the energy exchange at the reservoir-atmosphere interface. In this case, there is a different degree of energy-exchange intensification on both sides of the thermal bar. Due to the passage of the surface waters in the thermal bar area through the maximum density temperature, the total heat flux may change the direction on both sides of the thermal bar under certain hydrometeorological conditions. To the left of the TB, the heat flows contribute to intensification of the instability of the density of water masses as soon as the temperature of the surface waters approaches 4°C; to the right of the TB they cause its weakening. Under a long-term wind impact on the reservoir water area, this leads to weakening of near-shore circulation and deceleration of the TB distribution to the reservoir center.

ACKNOWLEDGMENTS

REFERENCES

1. K. Salonen, M. Pulkkanen, P. Salmi, and R. W. Griffiths, Limnol. Oceanogr. **59**, 2121 (2014). doi 10.4319/lo.2014.59.6.2121
2. P. Salmi and K. Salonen, Limnol. Oceanogr. **61**, 240 (2016). doi 10.1002/lno.10214
3. A. I. Tikhomirov, in *Temperature Conditions in Lake Onega* (Akad. Nauk SSSR, Leningrad, 1973), p. 202.
4. G. B. Kirillin, A. L. Forest, K. Graves, et al., Geophys. Rev. Lett. **42**, 2893 (2015). doi 10.1002/2014GL062180
5. P. R. Holland and A. Kay, Limnologica **33**, 153 (2003). doi 10.1016/S0075-9511(03)80011-7
6. N. S. Blokhina and K. V. Pokazeev, Zemlya Vselennaya, No. **6**, 78 (2015).
7. F. A. Forel, L'Echo Alpes, No. **3**, 149 (1880).
8. A. I. Tikhomirov, Izv. Vses. Geogr. O-va. **91**, 424 (1959).
9. A. I. Tikhomirov, Izv. Vses. Geogr. O-va. **95**, 134 (1963).
10. G. K. Rodgers, *Proc. 9th Conf. Great Lakes Res., Michigan, 1966*, p. 369.
11. N. S. Blokhina and A. E. Ordanovich, Moscow Univ. Phys. Bull. **67**, 109 (2012). doi 10.3103/S0027134912010031
12. J. Malm, PhD Thesis (Lund Univ., Lund, 1994).
13. V. Botte and A. A. Kay, Dyn. Atmos. Oceans **35**, 131 (2002). doi 10.1016/S0377-0265(01)00086-0
14. N. S. Blokhina and D. A. Solov'ev, Vestn. Mosk. Univ. Fiz. Astron., No. 3, 59 (2006).
15. D. A. Solov'ev and N. S. Blokhina, Oceanology **50**, 855 (2010). doi 10.1134/S0001437010060044
16. B. O. Tsydenov, A. Kay, and A. V. Starchenko, Ocean Modell. **104**, 73 (2016). doi 10.1016/j.ocemod.2016.05.009
17. D. M. Farmer and E. C. Carmack, J. Phys. Oceanogr. **11**, 1516 (1981).

18. N. S. Blokhina, Moscow Univ. Phys. Bull. **68**, 324 (2013). doi 10.3103/S0027134913040048

19. N. S. Blokhina, Moscow Univ. Phys. Bull. **70**, 319 (2015). doi 10.3103/S0027134915040050

20. N. S. Blokhina, Bull. Russ. Acad. Sci.: Phys. **81**, 96 (2017). doi 10.3103/S1062873817010099

21. N. S. Blokhina, A. E. Ordanovich, and O. S. Savel'eva, Water Resour. **28**, 201 (2001). doi 10.1023/A:1010339919712

22. N. S. Blokhina, A. V. Ovchinnikova, and A. E. Ordanovich, Moscow Univ. Phys. Bull. **57** (2), 73 (2002).

23. A. S. Monin and A. M. Yaglom, *Statistical Fluid Mechanics* (Nauka, Moscow, 1965), Vol. 1.

24. P. J. Roache, *Computational Fluid Dynamics* (Hermosa, Albuquerque, 1976).

25. A. S. Blokhin and N. S. Blokhina, Dokl. Akad. Nauk SSSR **193**, 805 (1970).

26. M. A. Naumenko, S. G. Karetnikov, E. M. Gorelova, and V. B. Rumyantsev, Izv. Vses. Geogr. O-va. **122**, 541 (1990).

27. M. A. Naumenko, V. V. Guzivaty, and S. G. Karetnikov, Oceanology **52**, 735 (2012). doi 10.1134/S0001437012060082

28. N. S. Blokhina, Water Resour. **41**, 379 (2014). doi 10.1134/S0097807814040034

Translated by L. Mukhortova